JARO 13: 745–758 (2012)
DOI: 10.1007/s10162-012-0342-3

JARO
Journal of the Association for Research in Otolaryngology

Research Article

Hyperpolarization-Activated Current (I_h) in Vestibular Calyx Terminals: Characterization and Role in Shaping Postsynaptic Events

Frances L. Meredith,[1] Tim A. Benke,[1,2,4,5] and Katherine J. Rennie[1,3,6]

[1]*Neuroscience Program, University of Colorado School of Medicine, Aurora, CO 80045, USA*

[2]*Department of Neurology, University of Colorado School of Medicine, Aurora, CO 80045, USA*

[3]*Department of Otolaryngology, University of Colorado School of Medicine, 12700 E. 19th Avenue, Aurora, CO 80045, USA*

[4]*Department of Pediatrics, University of Colorado School of Medicine, Aurora, CO 80045, USA*

[5]*Department of Pharmacology, University of Colorado School of Medicine, Aurora, CO 80045, USA*

[6]*Department of Physiology, University of Colorado School of Medicine, Aurora, CO 80045, USA*

Received: 5 April 2012; Accepted: 25 June 2012; Online publication: 24 July 2012

ABSTRACT

Calyx afferent terminals engulf the basolateral region of type I vestibular hair cells, and synaptic transmission across the vestibular type I hair cell/calyx is not well understood. Calyces express several ionic conductances, which may shape postsynaptic potentials. These include previously described tetrodotoxin-sensitive inward Na^+ currents, voltage-dependent outward K^+ currents and a K(Ca) current. Here, we characterize an inwardly rectifying conductance in gerbil semicircular canal calyx terminals (postnatal days 3–45), sensitive to voltage and to cyclic nucleotides. Using whole-cell patch clamp, we recorded from isolated calyx terminals still attached to their type I hair cells. A slowly activating, noninactivating current (I_h) was seen with hyperpolarizing voltage steps negative to the resting potential. External Cs^+ (1–5 mM) and ZD7288 (100 μM) blocked the inward current by 97 and 83 %, respectively, confirming that I_h was carried by hyperpolarization-activated, cyclic nucleotide gated channels. Mean half-activation voltage of I_h was −123 mV, which shifted to −114 mV in the presence of cAMP. Activation of I_h was well described with a third order exponential fit to the current (mean time constant of activation, τ, was 190 ms at −139 mV). Activation speeded up significantly (τ=136 and 127 ms, respectively) when intracellular cAMP and cGMP were present, suggesting that in vivo I_h could be subject to efferent modulation via cyclic nucleotide-dependent mechanisms. In current clamp, hyperpolarizing current steps produced a time-dependent depolarizing sag followed by either a rebound afterdepolarization or an action potential. Spontaneous excitatory postsynaptic potentials (EPSPs) became larger and wider when I_h was blocked with ZD7288. In a three-dimensional mathematical model of the calyx terminal based on Hodgkin–Huxley type ionic conductances, removal of I_h similarly increased the EPSP, whereas cAMP slightly decreased simulated EPSP size and width.

Keywords: HCN channel, balance, crista, cAMP, efferent

INTRODUCTION

Head motion and position are sensed by mechanosensitive hair cells embedded in sensory epithelia in the vestibular periphery. In amniotes, primary afferent neurons form three types of synaptic endings on hair cells. Calyx afferents form large, cup-shaped calyces that surround the basolateral region of one or more type I

Correspondence to: Katherine J. Rennie · Department of Otolaryngology · University of Colorado School of Medicine · 12700 E. 19th Avenue, Aurora, CO 80045, USA. Telephone: 1-303-7243070; fax:1-303-7241961; e-mail: katie.rennie@ucdenver.edu

hair cells. Bouton afferents contact type II hair cells. Dimorphic afferents branch to form calyx endings on type I hair cells and bouton terminals on type II cells. Action potential firing is spontaneous in these bipolar afferents. Firing pattern is either regular or irregular and corresponds to zonal differences in peripheral innervation (Baird et al. 1988; Goldberg 2000). Regularly firing afferents terminate in peripheral zones of vestibular sensory epithelia and irregularly firing afferents in more central zones (Goldberg 2000; Eatock and Songer 2011). Intrinsic membrane properties of afferent neurons may play an important role in determining firing pattern and ionic currents described in vestibular ganglion somata include voltage- and calcium-dependent K^+ currents (Chabbert et al. 2001a; Limón et al. 2005; Risner and Holt 2006; Iwasaki et al. 2008; Kalluri et al. 2010), sodium (Chabbert et al. 1997) and calcium currents (Desmadryl et al. 1997; Chambard et al. 1999; Autret et al. 2005), and a mixed cation hyperpolarization-activated current (I_h) (Chabbert et al. 2001b). Vestibular ganglion preparations lack peripheral dendritic terminals, but ionic conductances have also been described in the calyceal terminations of vestibular afferents (Hurley et al. 2006; Rennie and Streeter 2006; Dhawan et al. 2010; Meredith et al. 2011). Recent immunocytochemical work confirms the localization of several types of ion channel to the calyx (Lysakowski et al. 2011). The presence of these ion channels in calyx terminals infers important roles in coding afferent signals from presynaptic hair cells. Calyx endings also receive efferent signals from the brain, but the molecular mechanisms involved in efferent control of afferent signaling in the mammalian vestibular system remain largely unknown (Holt et al. 2011).

Hyperpolarization-activated, cyclic nucleotide gated (HCN) channels are widely expressed and give rise to an excitatory, noninactivating inward current (I_h). In mammals, there are four members of the HCN channel family (HCN1–4). Cyclic nucleotides interact directly with HCN channels through a C-terminal cyclic nucleotide binding domain (CNBD). cAMP increases conductance and shifts I_h voltage dependence to more depolarized potentials (DiFrancesco and Tortora 1991). I_h may influence integration of postsynaptic events by calibrating membrane resting potential and controlling membrane resistance.

I_h is prominent in auditory neurons, where it is typically active near the resting membrane potential and preserves timing information of acoustic signals by keeping excitatory postsynaptic potentials (EPSPs) brief and inhibiting summation of synaptic events (Bal and Oertel 2000). Within the vestibular periphery I_h has been found in hair cells of the frog sacculus, where it was speculated to play a role in restoring the resting potential after hyperpolarizations (Holt and Eatock 1995), bird semicircular canal (Masetto and Correia 1997; Masetto et al. 2000), and mouse utricle (Horwitz et al. 2011). Immunolabeling detected HCN1 in the basolateral region of hair cells and HCN2 and HCN4 in other neuroepithelial cells of the mouse utricle (Horwitz et al. 2010, 2011). This suggests that different HCN channel subtypes may predominate in presynaptic vestibular hair cells and postsynaptic afferent calyx terminals and implies specific roles for I_h in signal processing at the type I hair cell/calyx synapse.

Here, we provide the first electrophysiological characterization of I_h in vestibular calyx terminals. I_h has relatively fast activation kinetics and is blocked by Cs^+ and ZD7288. cAMP and cGMP accelerate I_h and cAMP shifts the activation curve to more positive potentials. As shown by our experimental and modeling work, I_h may influence postsynaptic events at the type I hair cell/calyx synapse by regulating action potentials and EPSPs.

METHODS

Whole-cell patch clamp was used to record from isolated single afferent calyx terminals in voltage and current clamp. Calyx endings and hair cells were isolated as described previously (Rennie and Streeter 2006; Dhawan et al. 2010). Calyx endings remained attached to type I hair cells. Voltage clamp recordings were also made from type II hair cells expressing I_h for a comparison of current activation kinetics (Fig. 4H).

Cell Isolation

The cristae ampullares of vestibular semicircular canals were surgically removed from male and female Mongolian gerbils (*Meriones unguiculatus*) at P3–P45 under deep anesthesia. Animal procedures followed protocols approved by the University of Colorado's Institutional Animal Care and Use Committee. Adult gerbils were anesthetized using intraperitoneal pentobarbitol sodium (Nembutal, 50 mg/kg) and intramuscular ketamine (10 mg/kg) and decapitated immediately following surgery. Early postnatal gerbils (up to P17, before eye-opening) were given Nembutal (50 mg/kg) and decapitated prior to removal of vestibular organs. Ampullae were placed directly in Leibovitz's L-15 medium (pH 7.40–7.45), osmolality 300–305 mmol/kg (distilled water) with bovine serum albumin (BSA, 0.5 mg/ml), and incubated for 30 min at 37 °C. Tissue was then kept at room temperature (21–24 °C) in fresh L-15 with BSA until recordings were made. In some experiments, ampullae were first placed in a high magnesium solution containing (in mM) NaCl (135), KCl (5), $MgCl_2$ (10), $CaCl_2$ (0.02),

HEPES (10), and D-glucose (3), pH 7.4 with NaOH and osmolality of 300–305 mmol/kg for 30 min at 37 °C prior to transferal to L-15 and BSA for a minimum of 50 min before plating. No difference was seen in the properties of the currents recorded from each treatment. Cell dissociation was performed without the use of exogenous enzymes. Instead, a fine stainless steel minutien pin (Fine Science Tools 26002-10) attached to a wooden probe was streaked across the epithelium of a crista in the recording chamber to mechanically dissociate cells. Cells were visualized with an Olympus upright microscope (BX50 or BX51 WI) with IR differential interference contrast optics.

Electrophysiological Recordings

Micropipette glass capillary tubes (PG165T outer diameter, 1.65 mm; inner diameter, 1.28 mm; Warner Instrument Corp., Hamden, CT, USA) were pulled on a horizontal micropipette puller (Sutter Instruments, San Rafael, CA, USA) and polished on a Narishige MF 830 microforge (Narishige International USA, East Meadow, NY, USA). The tips were coated with Silicone elastomer (Sylgard 184, Dow Corning, Midland, MI, USA). Patch electrode solution contained (in mM) KF (100), KCl (20), NaCl (2), HEPES (10), D-glucose (3), $MgCl_2$ (2), EGTA (10), MgATP (2), Li_xGTP (0.2), pH 7.4 with KOH (~29 mM), and osmolality of 300–305 mmol/kg (adjusted with mannitol). KF was included for recording stability. External solution was L-15. Open-tip patch pipette resistance ranged from 2.3 to 6.9 MΩ and gigaseals were obtained on the outer face of the calyx. Whole-cell voltage or current clamp recordings were made at room temperature (21–24 °C) following membrane rupture. Signals were amplified using an Axopatch-1D or Axopatch 200B patch amplifier (Molecular Devices, Sunnyvale, CA, USA) interfaced to a PC running pCLAMP (v8 or 10) through an AD converter (Digidata 1320A or 1440A, Molecular Devices). Data were low-pass filtered online at 2 or 5 kHz and sampled between 5 and 20 kHz, depending on the protocol used. Pipette capacitance and whole-cell capacitance were compensated in some recordings. Mean compensated capacitance for calyces was 2.78±0.20 pF (mean±SEM, n=48). Liquid junction potentials were calculated using the Junction Potential Calculator (Clampex 10) and corrected during data analysis. No leak subtraction was performed.

All chemicals were obtained from Sigma-Aldrich (St. Louis, MO, USA) except for 4-(*N*-ethyl-*N*-phenylamino)-1,2-dimethyl-6-(methylamino) pyrimidinium chloride (ZD7288) (Tocris Bioscience, Ellisville, MO, USA). A 20-mM stock of 8-bromoadenosine 3′,5′-cyclic monophosphate sodium salt (8-Br-cAMP) was made in distilled H_2O (dH_2O) and kept at −20 °C. On the day of the experiment, the stock was diluted in L-15 for a final concentration of 200 μM. For internal cAMP patch pipette solutions, a 10-mM stock of cAMP was made in dH_2O, stored at −20 °C and made up to a final concentration of 200 μM–1 mM in internal solution. A 25-mM cGMP stock was made in dH_20, stored at −20 °C, and made up to a final concentration of 200 μM in internal solution. A 10-mM stock of ZD7288 was made in dH_2O, stored at −20 °C and diluted in L-15 to a 50 or 100 μM final concentration on the day of the experiment. Cesium chloride (CsCl) and barium chloride were made up in L-15. Drugs were applied by rapid replacement of bath solution using a perfusion pipette. In some experiments, cells were perfused continuously at a rate of 0.5–1 ml/min using a peristaltic pump.

Data Analysis

Data were analyzed using pClamp 8 and 10 (Molecular Devices) and Sigmaplot 8, 11 or 12 (Systat Software). Statistical significance was determined using the Student's t test, Wilcoxon signed rank test or Mann–Whitney rank sum test, and values presented respectively as means±standard error of the mean (SEM) or medians.

Spontaneous excitatory postsynaptic potentials (EPSPs) were detected and analyzed using MiniAnalysis software (v 6.0.3, Synaptosoft, Decatur, GA, USA).

Mathematical Modeling of the Calyx

The three-dimensional passive and active membrane features of the vestibular calyx terminal were modeled in a novel fashion as a distributed parameter model (Halter and Clark 1991) by extending the formulation of the typical branched nerve equations (Hines 1984). The calyx membrane is divided into interconnected square membrane slabs (65 slabs; lengths, 1.5–3.2 μm) of 0.5 μm (near the apex) to 1.5 μm thickness (near the base); axial resistivity between slabs is maintained at 290 Ωcm. Membrane currents utilize Hodgkin–Huxley formulations, whereby sections of calyx membrane are characterized with a constant capacitance C (0.65×10^{-2} F/m^2) shunted by different ion channels (I_{Na}, I_h, I_A, I_D, and I_{leak}, which represent Na^+, hyperpolarization-activated, A-type, delayed rectifier and leak currents respectively). The potential V_j for the jth membrane slab is given by

$$dV_j/dt = 1/C\left(-\sum I_i + I_s\right) \quad (1)$$

where I_i represents the different ion channels. If present for that particular slab, I_s represents the externally applied current injected through a simulated patch electrode of fixed resistance, typically 1 MΩ

to simulate nearly fully cancelled access resistance. The current for different ion channels is $I_i = g_i(V - E_i)$, where g_i is the conductance and E_i is the reversal potential for each channel. Gating variables, solved using the Rush–Larson approximation (Hines 1984), for each channel are used to control the dynamics of activation and inactivation of each channel to scale maximum g_i. Steady-state activation, inactivation, time constants, maximal conductance, and reversal potential for each conductance are summarized in Tables 1 and 2 and are based on whole-cell calyx recordings from previously published (Rennie and Streeter 2006; Dhawan et al. 2010) and the current work; some represent minor modifications to prior formulations (Athanasiades et al. 2000). Conductances are assumed to be uniformly distributed throughout the calyx. Total capacitance for the simulated calyx was 5.9 pF and was based on a selected experimental calyx where whole-cell capacitance was not cancelled and the area under the capacitance transient was fit to accurately calculate the capacitance.

In order to determine how quantal transmission from type I hair cell activates the calyx, vesicular glutamate release from hair cell onto calyx AMPA receptor channels (AMPAR, n=100) is modeled with a kinetic scheme for GluA1 type receptors (Robert and Howe 2003). Channel openings in response to vesicular glutamate release (2 mM for 2 μs with 1 ms decay) are simulated macroscopically by a numerical solution to the system of equations described by the kinetic scheme using a fourth-order Runge–Kutta method. Resulting current due to channel openings is input into the model of the calyx above to simulate the effect of ionic conductances and calyx on the shape of EPSPs.

TABLE 2

Conductances and reversal potentials for Hodgkin Huxley formulations

Ion channel	*E_i (mV)*	*g_i, max (S/m^2)*
I_{Na}	108 = E_{Na}	45
I_h	−36	2.2
I_A	−83 = E_K	0.65
I_D	−83 = E_K	75
I_{leak}	−55, calculated to maintain V_{rest}	0.45

RESULTS

Calyx Afferent Terminals Show a Slow Inward, Hyperpolarization-Activated Current

Calyx terminals express voltage-dependent outward K^+ currents sensitive to 4-aminopyridine, tetraethylammonium and KCNQ channel blockers (Hurley et al. 2006; Rennie and Streeter 2006; Dhawan et al. 2010) and a K(Ca) current carried by small conductance (SK) channels (Meredith et al. 2011). In addition to the previously described inward Na^+ and outward K^+ conductances found in calyx terminals, prolonged voltage steps to hyperpolarized potentials also revealed the presence of a slowly-activating inward current (Meredith et al. 2011), which was further investigated here. Calyx terminals in this study

TABLE 1

Hodgkin Huxley formulations

Ion channel	*Conductance, g_i*	*Gating variable functions V (mV) and τ_i (ms)*	*References*
I_{Na}	$m^3h \times g_{Na}$	$m(V) = 1/(1 + \exp(-(V + 46)/2.14))$ $\tau_m(V) = (2.0/1,000.0)/(3.5 \times (0.36 \times (V + 55.0)/(1.0 - \exp(-(V + 55.0)/3.0)))$ $-0.4 \times (V + 73.0)/(1.0 - \exp((V + 73.0)/20.0))) + 0.05/1,000.0$ $h(V) = 1/(1 + \exp((V + 82)/4.71))$ $\tau_h(V) = (1.15 \times \exp(-0.055^2 \times (V + 49.6) \times (V + 49.6)) + 0.15)/1,000.0$	Rennie and Streeter 2006
I_h	$w^3 \times g_h$	$w(V) = 1.0/(1 + \exp((V + 124)/10.0))$ $\tau_w(V) = 3.768/(1.6 \times \exp(-(V + 54.0)/34.2) + 14.0/(0.7 + \exp(-(V + 40.0)/20.0)))$ $w_{cAMP}(V) = 1.0/(1 + \exp((V + 104)/15.0))$ $\tau_{w,cAMP}(V) = 6.3/(1.6 \times \exp(-(V + 54)/26.12) + 14.0/(0.7 + \exp(-(V + 40.0)/20.0)))$	This paper and Athanasiades et al. 2000
I_A	$p^3(q_1 + q_2) \times g_A$	$p(V) = 1.0/(1.0 + \exp(-(V + 54)/25))$ $\tau_p(V) = (5.5 \times \exp(-0.022^2 \times (V + 65.0) \times (V + 65.0)) + 1.0)/1,000.0$ $q_1(V) = 1.0/(1.0 + \exp((V + 70.0)/25))$ $\tau_{q1}(V) = 0.040$ $q_2(V) = 0.2 \times 1.0/(1.0 + \exp((V + 70.0)/25))$ $\tau_{q2}(V) = 0.1$	Dhawan et al. 2010
I_D	$x^3y \times g_D$	$x(V) = 1.0/(1.0 + \exp(-(V + 31.8)/13.1))$ $\tau_x(V) = (5.5 \times \exp(-0.022^2 \times (V + 65.0) \times (V + 65.0)) + 1.0)/1,000.0$ $y(V) = 1.0/(1.0 + \exp((V + 63.0)/4.7))$ $\tau_y(V) = 6.5$	Dhawan et al. 2010
I_{leak}	(fixed) g_{leak}	n/a	

had a mean zero current potential of −61.3±0.9 mV (n=79). In most experiments, we did not block the other conductances since their activation ranges do not overlap with I_h. At voltage steps to membrane potentials more hyperpolarized than −79 mV, a slowly developing inward current that increased in amplitude with increasingly negative voltage steps was seen. In the representative current traces in Figure 1A, instantaneous current (I_{ins}) was measured after the capacitance transient near the start of the voltage step. Currents continued to increase during the 650-ms voltage step. I_{end} indicates current measurement at the end of each voltage step. The tail currents following voltage steps were inward, indicating reversal more positive than the holding potential of −79 mV and a lack of selectivity for K^+ ions. Tail currents peaked within 40 ms, but were slow to deactivate (Fig. 1A, inset). The instantaneous and steady-state current–voltage relationships of the slowly activating inward currents are shown in the current–voltage (*IV*) plot (left panel) in Figure 1B. The difference ($I_{end}-I_{ins}$) reflects the current activated by hyperpolarization (right panel).

Mean $I_{end}-I_{ins}$ at −139 mV was −126.5±25.1 pA (n=9, Fig. 1C). Inward currents showed no inactivation, even when the step duration was increased to 2 s (Fig. 1D). Longer voltage steps were not well tolerated by calyces, and therefore, pulse duration was typically 650 ms. The hyperpolarization-activated current was observed in calyx terminals as early as P3, but most recordings presented here were from gerbils aged P21–45.

Hyperpolarizing current pulses injected in current clamp produced a steadily developing hyperpolarization followed by a slow, time-dependent depolarizing "sag" (Fig. 2A, B). The sag is a signature of cells expressing I_h and reflects the depolarization of membrane potential with hyperpolarization-activated inward currents. A depolarizing overshoot (Fig. 2A), or rebound spike (Fig. 2B), occurred at the end of the current pulse due to positive ions continuing to flow through HCN channels. The reversal potential of the hyperpolarization-activated current was estimated in voltage clamp by applying conditioning voltages to three different potentials followed by voltage ramps (Fig. 2C). The mean reversal potential was −35.5±

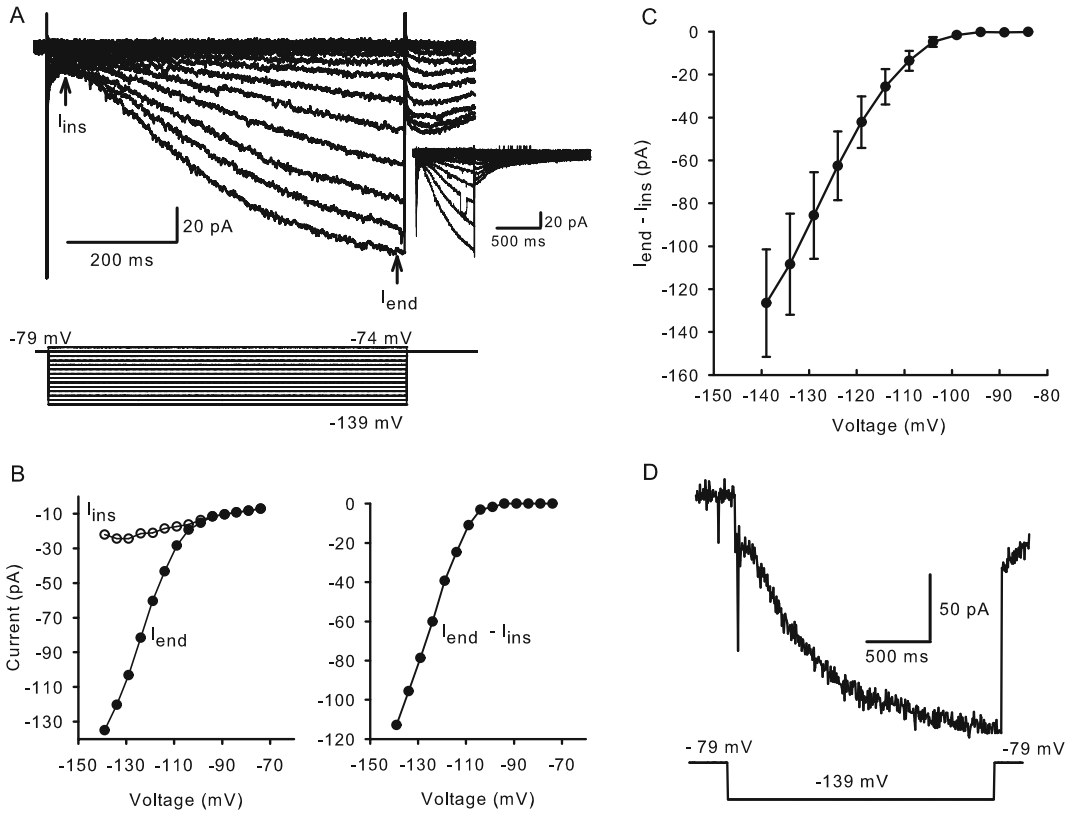

FIG. 1. Typical hyperpolarization-activated inward currents in calyx terminals. **A** Whole-cell currents elicited in response to hyperpolarizing steps in voltage clamp with voltage protocol shown below. The cell was held at −79 mV and stepped from −139 to −74 mV in incrementing 5 mV steps of 650 ms duration. A capacitive transient was followed by an instantaneous current (I_{ins}) at the start of the voltage step and a slowly developing inward current that approached steady state (I_{end}) towards the end of the step. At return to −79 mV, tail currents peaked within 40 ms. Tail currents are shown over a longer time course in a different cell (*inset*). **B** Instantaneous (*open circles*) and steady-state (*closed circles*) *IV* relationships for the cell in **A** (*left*). Current activated by hyperpolarization was obtained by subtracting I_{ins} from I_{end} (*right*). **C** *IV* relationship for $I_{end}-I_{ins}$ for nine calyx terminals (mean±SEM). **D** Hyperpolarization-activated current does not inactivate during a 2-s voltage pulse to −139 mV.

1.62 mV (n=4), which was slightly more positive than reversal potentials of −49 mV reported in primary vestibular neurons (Chabbert et al. 2001b) and −41 mV reported in spiral ganglion neurons (Mo and Davis 1997). In the majority of cells tested (six out of nine calyces), the current pulse was followed by a rebound spike (Figs. 2B and 5A). In the cell shown in Figure 2A, two hyperpolarizing current steps of 50 and 100 pA, each 100 ms in duration, evoked a sag response. The −100 pA current injection caused a more rapid hyperpolarization from rest and a faster onset of the depolarizing sag showing a time-dependent increase in I_h activation with increasing amplitude of hyperpolarizing currents.

I_h is carried by cations and the relative permeability of HCN channels to Na^+ and K^+ (P_{Na}/P_K) is reported to range from 1:3 to 1:5 (Biel et al. 2009). We therefore investigated the effect of raising extracellular K^+ on I_h. When K^+ was increased from 5.8 to 30 mM, hyperpolarization-activated currents increased substantially as expected for currents carried through HCN channels (Fig. 2D). Current following a step to −159 mV increased to 226±84.4 % (mean±SEM, n=3) compared to control.

Pharmacological Characterization of Hyperpolarization-Activated Currents

I_h is blocked by external Cs^+ and ZD7288 (Biel et al. 2009). Figure 3A shows block of the hyperpolarization-activated current in a calyx terminal by 1 mM Cs^+. The mean block in the presence of 1-5 mM Cs^+ was 97.3±0.99 % (n=9, Fig. 3C) and was partially reversible. In contrast, application of 0.5 mM Ba^{2+}, which blocks K^+-selective inward rectifier currents, did not reduce hyperpolarization-activated currents in three calyx terminals tested (data not shown).

ZD7288 is a nonselective blocker of HCN 1–4. Figure 3B shows the effect of two different concentrations of ZD7288 on a calyx terminal. Fifty micromolar of ZD7288 blocked ~20 % of the hyperpolarization-activated current, whereas 100 μM ZD7288 blocked the

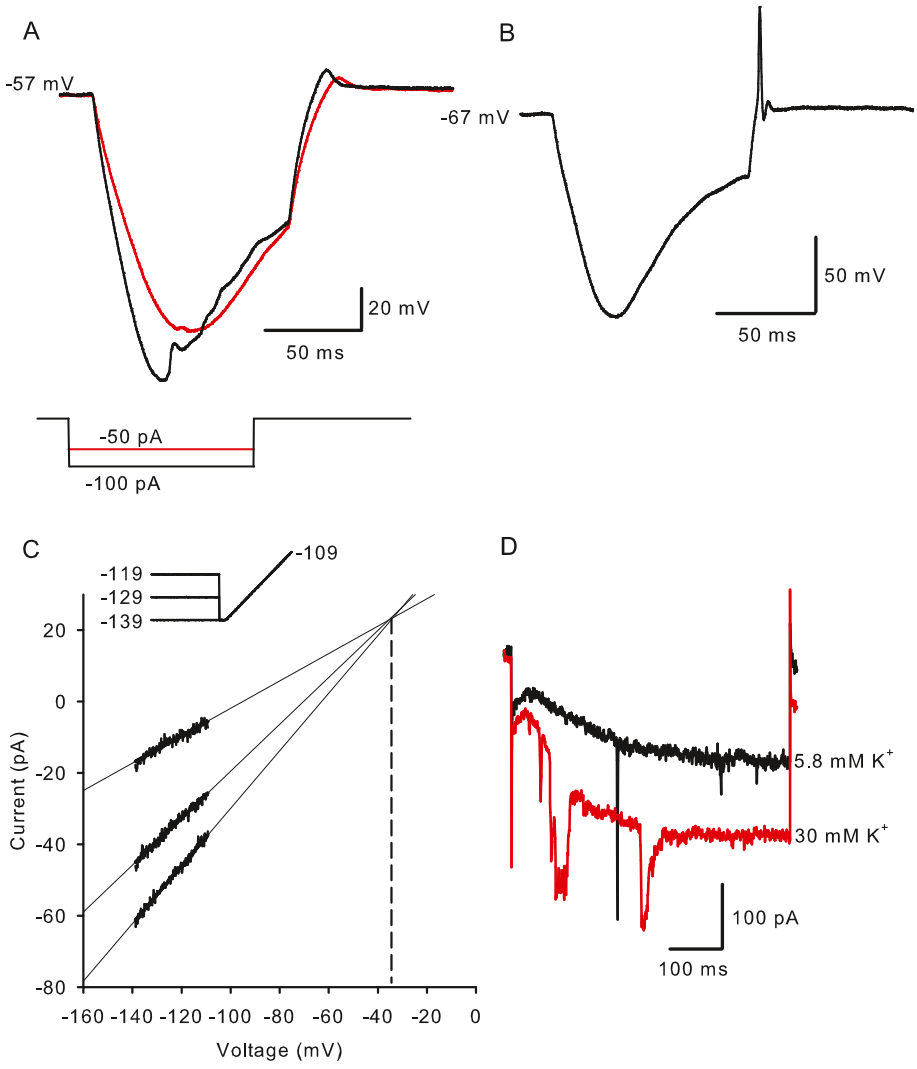

FIG. 2. Influence of I_h on membrane potential responses to current injections. **A** Hyperpolarizing current steps produced a time-dependent, depolarizing sag, returning the membrane potential towards its zero current potential of −57 mV. The amplitude of the sag varied with current amplitude, which was −50 pA (*red trace*) or −100 pA (*black trace*). A depolarizing overshoot occurred at the end of the current step. **B** In a different cell an action potential occurred at the termination of the −75 pA current step (zero current potential=−67 mV). **C** Reversal potential of I_h was estimated from extrapolation of current responses to 40 ms voltage ramps from −139 to −109 mV after conditioning voltages to −119, −129 and −139 mV for 1 s. Voltage commands are shown above the current responses. Current extrapolations intersected where conductance=0, i.e., the reversal potential which was −35.4 mV for the cell shown (*dashed line*). **D** Hyperpolarization-activated current increased when extracellular K^+ was raised from 5.8 mM (control, *black trace*) to 30 mM (*red trace*). Currents shown are in response to a voltage step from −79 to −159 mV.

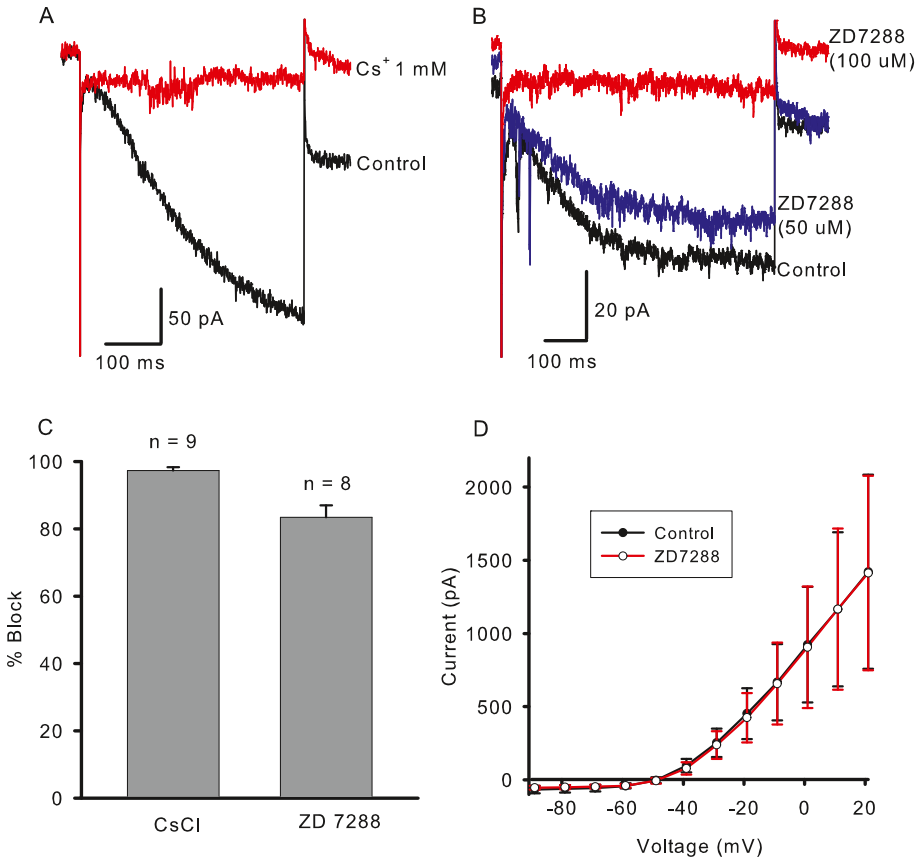

FIG. 3. Pharmacological characterization of I_h. **A** Inward current was blocked by extracellular application of 1 mM CsCl. Currents shown for voltage steps from −79 to −149 mV. **B** Block of I_h by ZD7288 was concentration dependent. $I_{end}-I_{ins}$ was reduced by 20 % in the presence of 50 μM ZD7288 and by 91 % in 100 μM ZD7288. Currents shown in response to a voltage step from −79 to −144 mV. The fast inward deflections seen on these and other records are likely excitatory postsynaptic currents (EPSCs) as described previously (Rennie and Streeter 2006; Yi et al. 2010). **C** Mean percent decrease in $I_{end}-I_{ins}$ amplitude was 97.3 % in the presence of 1–5 mM Cs^+ (n=9) and 83.3 % in 100 μM ZD7288 (n=8). **D** Mean outward potassium currents are unchanged after application of ZD7288 (n=3). Current amplitude was measured at the end of 40 ms voltage steps.

current by more than 90 %. The mean block in 100 μM ZD7288 was 83.3±3.6 % (n=8, Fig. 3C), which was slightly lower than that seen with Cs^+. Measurements of block were made within 1–13 min (mean, 4.4± 1.5 min) after ZD7288 application. In a previous study, a complete block of I_h required 10–15 min to take effect (Harris and Constanti 1995), suggesting that a more complete block in calyces would be expected with longer applications of the compound. The block by ZD7288 was also irreversible (data not shown) as described previously (Harris and Constanti 1995). ZD7288 (100 μM) was selective for I_h and did not block voltage-dependent outward K^+ currents in calyces (Fig. 3D, n=3).

Calyx Terminal I_h is Sensitive to Cyclic Nucleotides

HCN channels contain a CNBD that is sensitive to cAMP and cGMP. Binding of cyclic nucleotides relieves a block imposed by the CNBD on the channel, enabling it to open more rapidly. We tested the responses of I_h in calyces to cAMP using either membrane permeable 8-Br-cAMP in the extracellular solution or cAMP in the patch electrode solution. Application of external 200 μM 8-Br-cAMP enhanced I_h, and the effect in eight calyces is summarized in Figure 4A. The increase in current measured during a voltage step to −139 mV is shown for individual cells in Figure 4B. The control median (red line) increased significantly in the presence of 8-Br-cAMP.

We also compared I_h activation in control calyces to cells with cAMP included in the patch electrode solution (Fig. 4C). Measurement of peak tail currents following 5 mV steps was used to determine $V_{1/2}$ for calyx I_h. Activation curves were fitted using a Boltzmann function of the form

$$I/I_{max} = 1/1 + \exp\left[\left(V - V_{1/2}\right)/S\right] \qquad (2)$$

where V is the conditioning potential, $V_{1/2}$ is the half-maximum activation potential, and S determines the slope factor. cAMP produced a rightwards shift of the I_h activation curve. $V_{1/2}$ averaged −123.4±1.4 mV in control cells (n=5) and −113.9±0.8 mV in cells exposed to internal cAMP (n=7), whereas S (−10.5 mV) did not change (Fig. 4C).

I_h also increased in the presence of intracellular cGMP. Figure 4D shows currents in a calyx exposed to internal cGMP 2.5 min after the whole-cell configuration was attained (initial) and 15 min later when I_h had increased to a maximum value (final). The mean increase from −141.3±19.5 to −244.1±41.8 pA during a voltage step to −139 mV was significant (Fig. 4E, P=

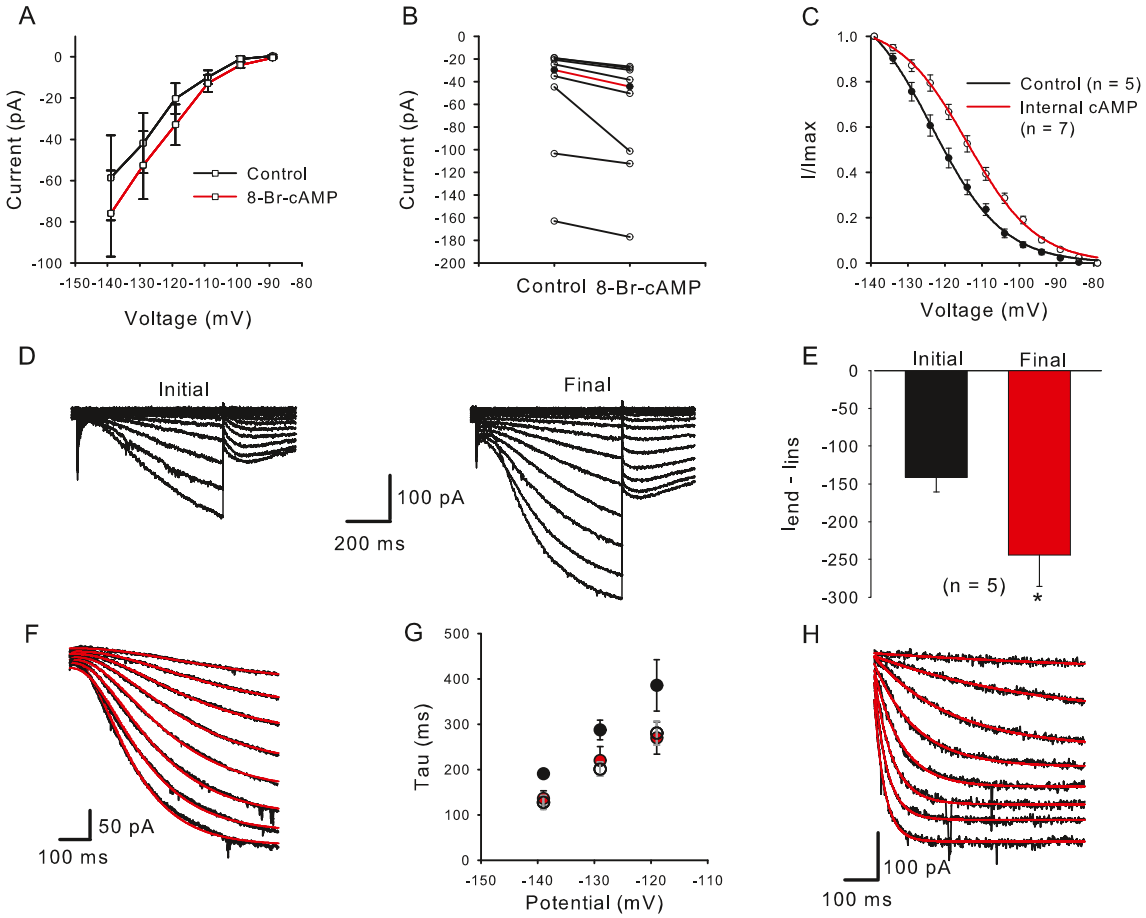

FIG. 4. Cyclic AMP and GMP increase I_h and shift its activation. **A** In the presence of external 8-Br-cAMP (data points connected by red line) mean $I_{end}-I_{ins}$ was larger at each voltage step compared to controls (*black line*). The mean current amplitude increased from −58.6 to −76.0 pA during a step to −139 mV (n=7). **B** Current values for eight cells are shown for control and 8-Br-cAMP. Median current amplitude (*red line*, $I_{end}-I_{ins}$) increased significantly from −29.9 to −44.4 pA at the −139 mV voltage step (P=0.008, n=8, Wilcoxon signed rank test). **C** Activation curves were obtained from control cells (no internal cAMP, *black line*) and in the presence of internal cAMP (*red line*). I/I_{max} was obtained from normalized tail currents and the means±SEM were plotted against prepulse voltage for controls (*closed circles*) and cAMP (*open circles*) and fitted with a Boltzmann function (Eq. 2). $V_{1/2}$ obtained from a fit to the mean data shifted from −123.4 mV (n=5) to −113.9 mV (n=7) with internal cAMP. **D** Whole-cell currents increased in the presence of 200 μM internal cGMP. **E** Mean current amplitude increased from an initial value of −141.3 to −244.1 pA after dialysis with cGMP. Control currents were measured within 2.5 min after breakthrough to the cell and final currents represent the maximum current reached. **F**, **G** cAMP and cGMP speed activation kinetics of I_h. **F** Representative current traces (*black*) to voltage steps from −144 to −109 mV (5 mV increments). The activation phase of I_h was fit with a single exponential with third order kinetics (Eq. 3) (*red lines*). **G** Mean time constants (tau) of activation for control cells (*black circles*, 14–28 cells) and cells exposed to internal cAMP (*red circles*, 3–5 cells) or cGMP (*unfilled circles*, 4 cells) for three different voltage steps. The time constant at the −139 mV step was significantly faster in the presence of internal cAMP (P=0.029; $n_{control}$=28; n_{cAMP}=5) and internal cGMP (P=0.013; n_{cGMP}=4), Mann–Whitney rank sum test. **H** Activation kinetics are faster in a type II hair cell. Voltage steps were from −164 to −94 mV (10 mV increments). Current activation was fit with a single exponential with first order kinetics (*red lines*). Tau for a step to −144 mV was 51.1 ms.

0.04, n=5) and was larger than that seen with internal cAMP (Fig. 4A, B). However, there was no significant shift in $V_{1/2}$ in the presence of cGMP (data not shown).

Activation of I_h Speeds Up in the Presence of Cyclic Nucleotides

The activation of I_h was clearly not instantaneous (Figs. 1A and 4D, F), suggesting that the kinetics of activation were greater than first order. Empirically, we found that I_h activation was best fitted with a cubed exponential equation of the form

$$I(t) = A[1 - \exp(-t/\tau)]^3 + A_0 \qquad (3)$$

in order to determine the time constant tau (τ). Figure 4F shows fits to control calyx I_h for membrane potential steps from –109 to –144 mV. Figure 4G shows the voltage dependence of τ for control cells

(black symbols) and cells where cAMP (red symbols) or cGMP (unfilled symbols) were included in the electrode solution. Mean values (±SEM) for a step to −139 mV were 190±8.7 ms for control cells (n=28), 135.9±17.3 ms (n=5) with internal cAMP, and 126.8±15.0 (n=4) with internal cGMP (Fig. 4G). The difference between control and cAMP- and cGMP-loaded cells was statistically significant (P=0.029 and P=0.013, respectively). For comparison, I_h was also recorded from gerbil semicircular canal type II hair cells (Fig. 4H), since HCN1 has recently been shown to underlie I_h in hair cells of the mouse utricle (Horwitz et al. 2011). The activation of I_h was much faster in type II hair cells compared with calyces (Fig. 4F, H), suggesting that subunits other than HCN1 are involved in calyx I_h. Mean τ was 60.2±14.3 ms (n=3) for a voltage step to −144 mV in gerbil type II hair cells, which is close to the mean value of 48 ms reported for the fast activation kinetics of I_h at −144 mV in wild-type hair cells of mouse utricle (Horwitz et al. 2011).

Effects of I_h in Current Clamp

Physiological roles of I_h in other cells include control of resting membrane potential, excitability, and rhythmicity. We therefore tested the effects of removing I_h on the zero current potential, action potential, and EPSPs in calyces. In ruptured and perforated patch clamp recordings from vestibular primary neurons, spontaneous action potentials are not usually observed, however, action potentials have been evoked in whole-cell current clamp in calyces (Rennie and Streeter 2006; Dhawan et al. 2010) and vestibular ganglion somata (Limón et al. 2005; Risner and Holt 2006; Iwasaki et al. 2008; Kalluri et al. 2010). We evoked action potentials by delivering repeated hyperpolarizing current injections in current clamp and also observed spontaneous EPSPs between action potentials (Fig. 5A). EPSPs occur in response to release of excitatory neurotransmitter (glutamate) from the presynaptic hair cell. To determine if I_h plays a role in shaping postsynaptic events, we recorded several EPSPs and action potentials before and after application of 100 μM ZD7288. The average EPSP became larger and wider following ZD7288 application (Fig. 5B), and a similar but smaller effect was seen on averaged action potentials (Fig. 5C). These results indicate that I_h can influence postsynaptic activity at physiologically relevant membrane potentials. We also found that the membrane resting potential became more hyperpolarized after application of ZD7288 (100 μM) from a mean of −56.6±3.7 to −60.2±3 mV (n=3, P=0.066, paired t test), but the difference was not significant.

Spontaneous firing was observed in a few calyces as shown in Figure 5D. Each action potential was followed by a membrane hyperpolarization to around −150 mV. This was sufficient to activate I_h as evidenced by the subsequent depolarizing sag. The mechanism underlying the membrane hyperpolarization is unknown, but would effectively remove sodium channel inactivation and activate I_h. The accompanying depolarization then leads to firing of an action potential.

Modeling I_h Contributions

We formulated a mathematical model of the calyx (see "Methods") to further probe the contributions of I_h. Membrane responses were simulated in voltage and current clamp under different conditions. We confirmed the ability of the model to simulate membrane ionic currents under voltage clamp conditions (Fig. 6). Outward K^+ currents and inward Na^+ currents (Fig. 6A) were similar to those we have previously reported (Rennie and Streeter 2006; Dhawan et al. 2010). Long duration hyperpolarizing steps [similar to experimental data, 0.5 s (cf. Fig. 1A)] were used to activate I_h from a holding potential of −79 mV (Fig. 6B). In additional simulations, step duration was extended to 2 s, and I_h activation kinetics (tau) and half-maximum activation potential ($V_{1/2}$) at 0.5 and 2 s were compared using similar step magnitude (not shown). Estimates of tau (cf. Fig. 4F) were unchanged, while estimates of $V_{1/2}$ were only 3 mV more hyperpolarized with the longer steps. This supports the accuracy of our experimental protocol to faithfully characterize I_h. Longer steps also produced significant inactivation of outward K^+ currents, which have contributions from I_A and I_D. Simulation of I_h in the presence of cAMP showed enhanced hyperpolarization-activated currents (Fig. 6B, right panel), similar to those seen with recorded calyx currents in Figure 4.

A series of hyperpolarizing steps in current clamp revealed passive membrane responses in the absence of I_h (Fig. 7A, left panel). Inclusion of the hyperpolarization-activated conductance to the model (Fig. 7A, middle panel) produced sag responses and poststep after depolarizations akin to those seen in experimental data (Fig. 2A). When cAMP-enhanced I_h was added, sag responses were modified accordingly. An EPSP was simulated at 0.35 s for all conditions (Fig. 7A). At the termination of the hyperpolarizing step a 200-pA depolarization was applied and evoked an action potential (Fig. 7B). Action potentials were similar under the different simulation conditions but showed a slight widening when I_h was not present (Fig. 7C), as seen experimentally. The EPSP was larger and slower when I_h was excluded (Fig. 7D), as seen in Figure 5B with averaged experimental EPSPs. cAMP further decreased the width and peak of the simulated EPSP suggesting physiological modulation of EPSPs could occur via a cAMP-dependent mechanism.

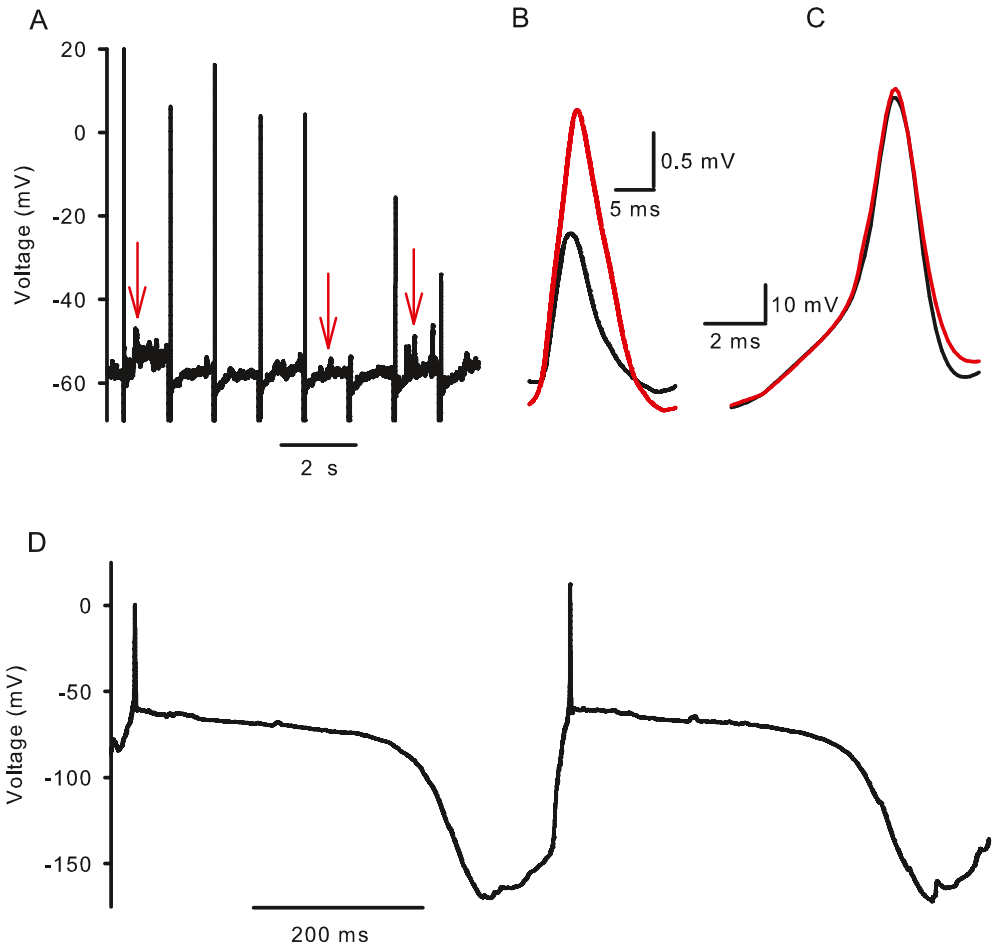

FIG. 5. ZD7288 and synaptic potentials in calyx afferents. **A** Evoked action potentials and spontaneous EPSPs recorded in current clamp in a calyx terminal. Action potentials typically occurred in response to (−100 pA, 20 ms duration) current injections presented every 1.2 s. Between spikes EPSPs were observed as upward deflections from rest (examples indicated by *red arrows*). **B** EPSPs were averaged before (*black trace*) and after (*red trace*) application of 100 μM ZD7288 to block I_h. Averages of a total of 171 events from three cells are shown. ZD7288 broadened mean EPSP width and increased the amplitude. **C** Action potentials were averaged before (21 action potentials, *black trace*) and after (17 action potentials, *red trace*) application of 100 μM ZD7288. **D** Spontaneous action potentials recorded in current clamp in a calyx terminal are followed by a slow hyperpolarization and subsequent depolarization to action potential threshold.

DISCUSSION

Hair bundle deflection modulates action potential firing in vestibular afferents. In amniotes, type I hair cells make ribbon synapses with highly specialized calyx terminals, which engulf the basolateral portion of the type I hair cell. Recent immunocytochemical data show several different types of ion channel are present on the inner and outer faces of calyx endings (Lysakowski et al. 2011), suggesting active roles in the initiation and processing of synaptic signals. To date, tetrodotoxin-sensitive voltage-dependent inward Na^+ currents, outward K^+ currents sensitive to 4-aminopyridine, tetraethylammonium, and the KCNQ channel blockers linopirdine and XE991 (Hurley et al. 2006; Rennie and Streeter 2006; Dhawan et al. 2010), and a K(Ca) current sensitive to apamin and nifedipine (Meredith et al. 2011) have been described in calyx terminals. Here, we have characterized an additional inwardly rectifying current with hallmarks of I_h. The current shows relatively slow, voltage-dependent activation at hyperpolarized membrane potentials, is blocked by external Cs^+ and ZD7288 and enhanced by raising extracellular K^+ or application of cAMP and cGMP. Both experimental and simulated data show that I_h modulates the shape of calyx EPSPs and may therefore be important for transmission of vestibular signals.

I_h Properties—Magnitude and Voltage Range of Activation

The magnitude of I_h and the voltage range at which it is activated determine its contribution to input resistance and its effects on membrane excitability. The voltage range of I_h activation varies markedly between different cell types. $V_{1/2}$ for I_h in adult guinea pig spiral ganglion neurons was between −110 and −120 mV (Chen 1997)

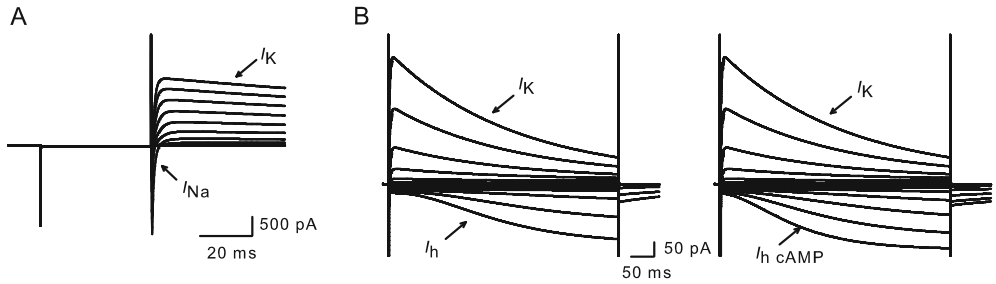

FIG. 6. Modeling voltage-dependent current in calyx terminals. **A** Currents were simulated in response to a voltage protocol from a holding potential of −79 mV, followed by a 40-ms prepulse to −129 mV and subsequent test steps from −89 to +19 mV in 10-mV increments. Rapid inward sodium currents (I_{Na}) and macroscopic outward potassium currents (I_K) resemble those described previously (Dhawan et al. 2010). **B** Longer duration voltage steps (0.5 s) evoke I_h at hyperpolarized voltage steps (*left*). Steps were applied from a holding potential of −79 mV between −149 and −19 mV in 10-mV increments. cAMP in conjunction with I_h increased the size and accelerated the activation of the inward currents (*right*).

and was about −104 mV in rat primary auditory afferent dendrites (Yi et al. 2010). $V_{1/2}$ for I_h in early postnatal (P5-P8) mouse primary vestibular ganglion cells averaged −110 mV (Chabbert et al. 2001b), and we found a mean $V_{1/2}$ of −123 mV in control gerbil calyces. Therefore, I_h is substantially activated at potentials more hyperpolarized than the mean resting potential, which averaged −61 mV in our isolated calyx terminals and −68 mV in vestibular ganglion neurons (Kalluri et al. 2010). Relatively hyperpolarized $V_{1/2}$ values have also been reported in rat olfactory sensory neurons (−142 and −117 mV, Lynch and Barry 1991; Vargas and Lucero 1999) and mouse vomeronasal sensory neurons (−118 mV, Dibattista et al. 2008). $V_{1/2}$ values are influenced by recording temperature, pulse protocol duration, and the intracellular environment (Wahl-Schott and Biel 2009). For example, alteration of Ca^{2+} levels during whole-cell recordings shifts activation of I_h (Hagiwara and Irisawa 1989; Schwindt et al. 1992; Mo and Davis 1997) and phosphatidylinositol 4,5 bishosphate (PIP_2) washout may cause I_h rundown (Wahl-Schott and Biel 2009).

Recent electrophysiological studies on isolated rat ganglion somata implicated low-voltage-activated K^+ currents (I_{LV}) in regulation of spike timing in

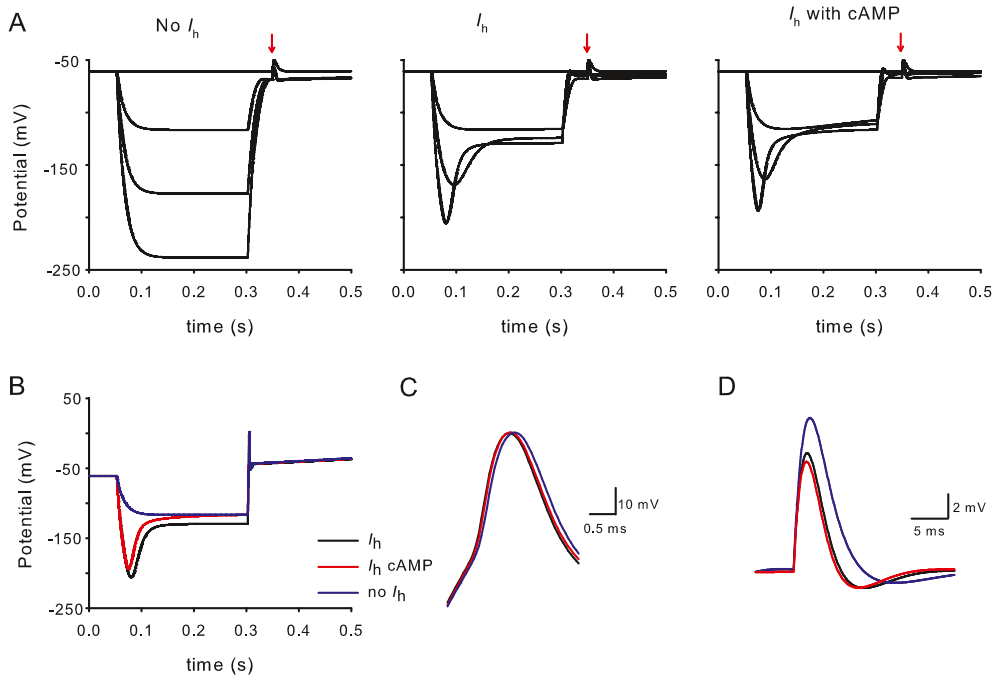

FIG. 7. Modeling calyx terminal responses in current clamp to probe I_h contributions. **A** Response of calyx terminal at rest and to a series of hyperpolarizing steps (25, 50, and 75 pA) from −61 mV with conductances as described in Table 2 but lacking I_h (*left*), same protocol with I_h added (*middle*) and with I_h in the presence of cAMP (*right*). A simulated EPSP in response to a glutamate pulse is presented at 0.35 s (*arrows*). **B** Response to hyperpolarizing steps from −61 mV with no I_h (−25 pA, *blue trace*), I_h included (−75 pA, *black*) and I_h with cAMP (−75 pA, *red*). A depolarizing step (200 ms duration) of 200 pA at the termination of the pulse evokes an action potential. **C** Detail of action potential in B aligned to mean zero current potential with no I_h (*blue trace*), I_h included (*black*), and I_h with cAMP (*red*). **D** Simulated calyx EPSP with no I_h (*blue*), I_h included (*black*), and I_h with cAMP (*red*).

vestibular afferents (Iwasaki et al. 2008; Kalluri et al. 2010). Vestibular ganglion neurons showed transient or sustained action potential responses following depolarizing current steps. Transient neurons in ganglion somata fired one or two action potentials to depolarizing current steps and may correspond to irregularly firing calyx afferents (Kalluri et al. 2010). Sag responses occurred with hyperpolarizing current steps in current clamp, and the sag peak increased with increasing step size (Kalluri et al. 2010). Action potentials often followed the sag at the offset of the hyperpolarizing stimulus in ganglion cells (Kalluri et al. 2010) and were also seen in calyx terminals (Fig. 2B). Sustained neurons, which may correspond to regular afferents, showed a more prominent sag and were more likely to spike at stimulus end (Kalluri et al. 2010). Although contributions from HCN channels were not studied directly, it was suggested that I_h could depolarize ganglion cell resting potential, thereby increasing the activation of I_{LV} to induce a more transient firing pattern (Kalluri et al. 2010). I_{LV} in transient vestibular ganglion cells was reduced by the Kv1 channel blocker α-dendrotoxin (Iwasaki et al. 2008; Kalluri et al. 2010). However, we previously found no evidence for an α-dendrotoxin-sensitive current in isolated calyces (Dhawan et al. 2010). Here, we have demonstrated the presence of I_h in calyces and examined its role in membrane responses at the afferent synaptic terminals. The relative contribution of I_h in ganglion cell bodies and bouton terminals innervating type II hair cells remains to be elucidated.

Pharmacology of I_h

I_h in this study was blocked by Cs^+ (97.3 %) and the more selective blocker ZD7288 (83.3 %). Cs^+ can also block the K^+-selective inward rectifier current, I_{Kir}, which has rapid activation and inactivation kinetics. I_{Kir} was reported in pigeon semicircular hair cells and supporting cells (Masetto and Correia 1997) and in mouse utricular hair cells (Rüsch and Eatock 1996). In vestibular ganglion cells Ba^{2+}, which blocks I_{Kir} but not I_h, abolished an early portion of the hyperpolarization-activated current, suggesting a contribution from I_{Kir} (Chabbert et al. 2001b). Correia et al. (2004) found pKir2.1 channel expression, which could underlie I_{Kir}, in pigeon vestibular ganglion somata but not in calyx terminals. In agreement with this, we saw no evidence for a fast inward rectifier in mammalian calyces. We observed a reduction in instantaneous current in response to ZD7288 (Fig. 3B), but not to Cs^+ (Fig. 3A). The difference in sensitivities has been attributed to at least two open states for HCN2 channels, one a "leaky" open state permeable to Cs^+ and the other a "normal" hyperpolarization-activated state sensitive to Cs^+ (Proenza et al. 2002).

Modulation by cAMP and cGMP

Of the four HCN homotetramers, HCN2 and HCN4 have the most hyperpolarized $V_{1/2}$ values (−70 to −100 mV) and a similar sensitivity to cAMP, but HCN2 has faster activation kinetics. In this study, the rightward shift in $V_{1/2}$ of ~9 mV in calyces exposed to internal cAMP, coupled with the relatively fast activation kinetics (τ, ~190 ms) at −139 mV suggest involvement of HCN2 subunits. This is consistent with the detection of HCN2 immunoreactivity in afferent neurons of the mouse utricle (Horwitz et al. 2010) and contrasts with the three- to fourfold faster activation kinetics of I_h in type II hair cells reported here and in hair cells of the mouse utricle, where HCN1 isoforms are predominantly expressed (Horwitz et al. 2011). HCN2 isoforms give rise to slower currents than HCN1, but currents are faster than those seen with HCN3 and HCN4. Sensitivity of I_h to cAMP has not previously been investigated in the peripheral vestibular system, but the shift in $V_{1/2}$ reported here is higher than the ~2–3 mV shift in spiral ganglion cells (Chen 1997), but similar to the ~12 mV shift seen in primary auditory dendrites where HCN subunits 1, 2, and 4 were expressed (Yi et al. 2010). Cyclic nucleotides relieve a block imposed by the CNBD on the channel, enabling it to open more rapidly. The block is thought to be greater in HCN2 than HCN1 channels, accounting for the larger depolarizing shift in activation and faster opening kinetics in HCN2 channels in response to cAMP (Wainger et al. 2001). Intracellular cGMP did not cause a significant shift in $V_{1/2}$, but accelerated the activation kinetics of I_h and increased current amplitude by more than 50 %.

Is I_h Modulated by Efferent Neurotransmitters?

Efferent fibers terminate on the outer faces of calyx afferents and could release neurotransmitters regulating I_h. Electrical stimulation of the efferent system leads to an increase in firing in mammalian vestibular afferents and calyx units show the largest responses to efferent stimulation (reviewed in Holt et al. 2011). ACh is thought to be a major efferent neurotransmitter, but other candidate transmitter molecules include ATP, calcitonin gene-related peptide, opioid peptides, γ-aminobutyric acid, nitric oxide, and dopamine (Drescher et al. 2010; Holt et al. 2011). Efferent transmitters could potentially influence I_h gating by modulating intracellular levels of cyclic nucleotides. HCN channels can be potentiated by direct binding of cAMP through the CNBD and intracellular cAMP levels could change via G-protein-coupled inhibition or activation of adenylyl cyclase. cAMP can also shift activation positively by PKA-mediated channel phosphorylation (Liao et al. 2010). Our data show that cGMP is a potent modulator of I_h, and in vivo cGMP levels could be modulated through nitric oxide activation

of guanylyl cyclase (Garthwaite 2008). Dopamine is found in auditory efferents (Gáborján et al. 1999), and immunoreactivity for dopamine receptor subtypes D1A and D2L was reported on both inner and outer faces of calyces from the rat saccule and mouse utricle (Drescher et al. 2010). It is tempting to speculate that elevating levels of intracellular cyclic nucleotides could enhance firing in calyx afferents through I_h; however, further experiments are required to provide a possible direct link between I_h modulation and efferent input to the calyx.

Regulation of I_h by Extracellular K^+

The extracellular milieu may also play a significant role in regulating I_h in calyx terminals. The intercellular cleft between the type I hair cell and calyx is restricted and K^+ levels in the synaptic cleft may fluctuate. Hair cell inhibition could cause a reduction in intercellular cleft levels of K^+, whereas levels could rise substantially during depolarization of the type I hair cell through efflux of K^+ via hair cell basolateral K^+ channels (Goldberg 1996; Rennie and Correia 2000; Lim et al. 2011). I_h is a mixed Na^+/K^+ current with an approximately fourfold greater permeability for K^+ over Na^+ under normal conditions. Increasing extracellular K^+ concentration enhances I_h and also slightly decreases the selectivity for K^+ over Na^+ (Biel et al. 2009; Frace et al. 1992). In rabbit sinoatrial node cells, removal of K^+ from the extracellular solution reduced I_h to negligible levels, whereas increasing K^+ greatly augmented I_h (Frace et al. 1992). We have confirmed that I_h amplitude in calyces increases with an increase in bath K^+ (Fig. 2D). I_h would serve to remove excess K^+ if the calyx did not depolarize substantially. Although HCN2 and HCN4 have been reported in vestibular afferent neurons (Horwitz et al. 2010), the precise localization of HCN channels on the calyx terminal is not yet known. In our current model, they are evenly distributed, but channels could be present on the outer face of the calyx, adjacent to efferent terminals and/or on the inner face of the calyx adjacent to the type I hair cell.

Effect of I_h on EPSPs and Membrane Excitability

It is important to identify ionic conductances that influence the resting membrane potential, especially in neurons that are spontaneously active such as vestibular afferents. Although the relationship between EPSPs and spike generation in vestibular terminals is not yet clear, large EPSPs with rapid onset kinetics are expected to trigger action potentials. Similar to auditory afferents, vestibular afferent synapses appear specialized for the rapid and reliable transmission of mechanosensory signals and exhibit phase locking to stimulus frequency (McCue and Guinan 1994). In response to repeated sinusoidal hair bundle deflections, calyceal EPSPs showed adaptation (Eatock and Songer 2011). We found that blocking I_h with ZD7288 resulted in a small hyperpolarization of the membrane potential, suggesting that membrane excitability in calyces may change when I_h is modulated. Although ZD7288 (100 μM) had no effect on evoked action potentials in mouse vestibular ganglion neurons (Chabbert et al. 2001b), we observed a small increase in peak and width of simulated and actual action potentials following removal of I_h (Figs. 5C and 7C). In cochlear afferent dendrites, I_h served to shorten EPSPs and blocking I_h with ZD7288 increased action potential half-widths (Yi et al. 2010). We removed I_h with ZD7288 in patch clamp recordings and from the mathematical model of the calyx. In both experimental and simulation conditions, I_h removal changed the shape of EPSPs by increasing the peak and width. This infers that I_h sharpens the postsynaptic response and enhances temporal precision of vestibular signals.

ACKNOWLEDGMENTS

This work was supported by National Institute on Deafness and other Communication Disorders (NIDCD) Grant DC-008297 and an American Otological Society Grant to KJR. FLM was partly supported by 5T32NS007083. We thank Tommy Bui for excellent technical assistance.

REFERENCES

ATHANASIADES A, CLARK JW JR, GHORBEL F, BIDANI A (2000) An ionic current model for medullary respiratory neurons. J Comput Neurosci 9:237–257

AUTRET L, MECHALY I, SCAMPS F, VALMIER J, LORY P, DESMADRYL G (2005) The involvement of $Ca_V3.2/\alpha1H$ T-type calcium channels in excitability of mouse embryonic primary vestibular neurones. J Physiol 567:67–78

BAIRD RA, DESMADRYL G, FERNANDEZ C, GOLDBERG JM (1988) The vestibular nerve of the chinchilla. I. Peripheral innervation patterns in the horizontal and superior semicircular canals. J Neurophysiol 60:182–203

BAL R, OERTEL D (2000) Hyperpolarization-activated, mixed-cation current ($I(_h)$) in octopus cells of the mammalian cochlear nucleus. J Neurophysiol 84:806–817

BIEL M, WAHL-SCHOTT C, MICHALAKIS S, ZONG X (2009) Hyperpolarization-activated cation channels: from genes to function. Physiol Rev 89:847–885

CHABBERT C, CHAMBARD JM, VALMIER J, SANS A, DESMADRYL G (1997) Voltage-activated sodium currents in acutely isolated mouse vestibular ganglion neurones. Neuroreport 8:1253–1256

CHABBERT C, CHAMBARD JM, SANS A, DESMADRYL G (2001a) Three types of depolarization-activated potassium currents in acutely isolated mouse vestibular neurons. J Neurophysiol 85:1017–1026

CHABBERT C, CHAMBARD JM, VALMIER J, SANS A, DESMADRYL G (2001b) Hyperpolarization-activated (I_h) current in mouse vestibular primary neurons. Neuroreport 12:2701–2704

CHAMBARD JM, CHABBERT C, SANS A, DESMADRYL G (1999) Developmental changes in low and high voltage-activated calcium currents in acutely isolated mouse vestibular neurons. J Physiol 518:141–149

CHEN C (1997) Hyperpolarization-activated current (I_h) in primary auditory neurons. Hear Res 110:179–190

CORREIA MJ, WOOD TG, PRUSAK D, WENG T, RENNIE KJ, WANG HQ (2004) Molecular characterization of an inward rectifier channel (I_{Kir}) found in avian vestibular hair cells: cloning and expression of pKir2.1. Physiol Genomics 19:155–169

DESMADRYL G, CHAMBARD JM, VALMIER J, SANS A (1997) Multiple voltage-dependent calcium currents in acutely isolated mouse vestibular ganglion neurons. Neuroscience 78:511–522

DHAWAN R, MANN SE, MEREDITH FL, RENNIE KJ (2010) K^+ currents in isolated vestibular afferent calyx terminals. J Assoc Res Otolaryngol 11:463–476

DIBATTISTA M, MAZZATENTA A, GRASSI F, TIRINDELLI R, MENINI A (2008) Hyperpolarization-activated cyclic nucleotide-gated channels in mouse vomeronasal sensory neurons. J Neurophysiol 100:576–586

DIFRANCESCO D, TORTORA P (1991) Direct activation of cardiac pacemaker channels by intracellular cyclic AMP. Nature 351:145–147

DRESCHER MJ, CHO WJ, FOLBE AJ, SELVAKUMAR D, KEWSON DT, ABU-HAMDAN MD, OH CK, RAMAKRISHNAN NA, HATFIELD JS, KHAN KM, ANNE S, HARPOOL EC, DRESCHER DG (2010) An adenylyl cyclase signaling pathway predicts direct dopaminergic input to vestibular hair cells. Neuroscience 171:1054–1074

EATOCK RA, SONGER JE (2011) Vestibular hair cells and afferents: two channels for head motion signals. Annu Rev Neurosci 34:501–534

FRACE AM, MARUOKA F, NOMA A (1992) External K^+ increases Na^+ conductance of the hyperpolarization-activated current in rabbit cardiac pacemaker cells. Pflugers Arch 421:97–99

GÁBORJÁN A, LENDVAI B, VIZI ES (1999) Neurochemical evidence of dopamine release by lateral olivocochlear efferents and its presynaptic modulation in guinea-pig cochlea. Neuroscience 90:131–138

GARTHWAITE J (2008) Concepts of neural nitric oxide-mediated transmission. Eur J Neurosci 11:2783–2802

GOLDBERG JM (1996) Theoretical analysis of intercellular communication between the vestibular type I hair cell and its calyx ending. J Neurophysiol 76:1942–1957

GOLDBERG JM (2000) Afferent diversity and the organization of central vestibular pathways. Exp Brian Res 130:277–297

HAGIWARA N, IRISAWA H (1989) Modulation by intracellular Ca^{2+} of the hyperpolarization-activated inward current in rabbit single sino-atrial node cells. J Physiol 409:121–141

HALTER JA, CLARK JW JR (1991) A distributed-parameter model of the myelinated nerve fiber. J Theor Biol 148:345–382

HARRIS NC, CONSTANTI A (1995) Mechanism of block by ZD 7288 of the hyperpolarization-activated inward rectifying current in guinea pig substantia nigra neurons in vitro. J Neurophysiol 74:2366–2378

HINES ML (1984) Efficient computation of branched nerve equations. Int J Bio-Med Computing 15:69–76

HOLT JR, EATOCK RA (1995) Inwardly rectifying currents of saccular hair cells from the leopard frog. J Neurophysiol 73:1484–1502

HOLT JC, LYSAKOWSKI A, GOLDBERG JM (2011) The efferent vestibular system. In: Ryugo DD, Fay RR, Popper AN (eds) Auditory and vestibular efferents. Springer, New York, pp 135–186

HORWITZ GC, LELLI A, GELEOC GS, HOLT JR (2010) HCN channels are not required for mechanotransduction in sensory hair cells of the mouse inner ear. PLoSone 5:1–7

HORWITZ GC, RISNER-JANICZEK JR, JONES SM, HOLT JR (2011) HCN channels in the inner ear are necessary for normal balance function. J Neurosci 31:16814–16825

HURLEY KM, GABOYARD S, ZHONG M, PRICE SD, WOOLTORTON JRA, LYSAKOWSKI A, EATOCK RA (2006) M-like K^+ currents in type I hair cells and calyx afferent endings of the developing rat utricle. J Neurosci 40:10253–10269

IWASAKI S, CHIHARA Y, KOMUTA Y, ITO K, SAHARA Y (2008) Low-voltage-activated potassium channels underlie the regulation of intrinsic firing properties of rat vestibular ganglion cells. J Neurophysiol 100:2192–2204

KALLURI R, XUE J, EATOCK RA (2010) Ion channels set spike timing regularity of mammalian vestibular afferent neurons. J Neurophysiol 104:2034–2051

LIAO Z, LOCKHEAD D, LARSON ED, PROENZA C (2010) Phosphorylation and modulation of hyperpolarization-activated HCN4 channels by protein kinase A in the mouse sinoatrial node. J Gen Physiol 136:247–258

LIM R, KINDIG AE, DONNE SW, CALLISTER RJ, BRICHTA AM (2011) Potassium accumulation between type I hair cells and calyx terminals in mouse crista. Exp Brain Res 210:607–621

LIMÓN A, PÉREZ C, VEGA R, SOTO E (2005) Ca^{2+}-activated K^+-current density is correlated with soma size in rat vestibular-afferent neurons in culture. J Neurophysiol 94:3751–3761

LYNCH JW, BARRY PH (1991) Inward rectification in rat olfactory receptor neurons. Proc Biol Sci 243:149–153

LYSAKOWSKI A, GABOYARD-NIAY S, CALIN-JAGEMAN I, CHATLANI S, PRICE SD, EATOCK RA (2011) Molecular microdomains in a sensory terminal, the vestibular calyx ending. J Neurosci 31:10101–10114

MASETTO S, CORREIA MJ (1997) Electrophysiological properties of vestibular sensory and supporting cells in the labyrinth slice before and during regeneration. J Neurophysiol 78:1913–1927

MASETTO S, PERIN P, MALUSÀ A, ZUCCA G, VALLI P (2000) Membrane properties of chick semicircular canal hair cells in situ during embryonic development. J Neurophysiol 83:2740–2756

MCCUE MP, GUINAN JJ (1994) Influence of efferent stimulation on acoustically responsive vestibular afferents in the cat. J Neurosci 14:6071–6083

MEREDITH FL, LI G, RENNIE KJ (2011) Postnatal expression of an apamin-sensitive K(Ca) current in vestibular calyx terminals. J Memb Biol 244:81–91

MO Z-L, DAVIS RL (1997) Heterogeneous voltage dependence of inward rectifier currents in spiral ganglion neurons. J Neurophysiol 78:3019–3027

PROENZA C, ANGOLI D, AGRANOVICH E, MACRI V, ACCILI EA (2002) Pacemaker channels produce an instantaneous current. J Biol Chem 277:5101–5109

RENNIE KJ, CORREIA MJ (2000) Effects of cationic substitutions on delayed rectifier current in type I vestibular hair cells. J Membr Biol 173:139–148

RENNIE KJ, STREETER MA (2006) Voltage-dependent currents in isolated vestibular afferent calyx terminals. J Neurophysiol 95:26–32

RISNER JR, HOLT JR (2006) Heterogeneous potassium conductances contribute to the diverse firing properties of postnatal mouse vestibular ganglion neurons. J Neurophysiol 96:2364–2376

ROBERT A, HOWE JR (2003) How AMPA receptor desensitization depends on receptor occupancy. J Neurosci 23:847–858

RÜSCH A, EATOCK RA (1996) Voltage responses of mouse utricular hair cells to injected currents. Ann N Y Acad Sci 781:71–84

SCHWINDT PC, SPAIN WJ, CRILL WE (1992) Effects of intracellular calcium chelation on voltage-dependent and calcium-dependent currents in cat neocortical neurons. Neuroscience 47:571–578

VARGAS G, LUCERO MT (1999) Dopamine modulates inwardly rectifying hyperpolarization-activated current (I_h) in cultured rat olfactory receptor neurons. J Neurophysiol 81:149–159

WAHL-SCHOTT C, BIEL M (2009) HCN channels: structure, cellular regulation and physiological function. Cell Mol Life Sci 66:470–494

WAINGER BJ, DEGENNARO M, SANTORO B, SIEGELBAUM SA, TIBBS GR (2001) Molecular mechanisms of cAMP modulation of HCN pacemaker channels. Nature 411:805–810

YI E, ROUX I, GLOWATZKI E (2010) Dendritic HCN channels shape excitatory postsynaptic potentials at the inner hair cell afferent synapse in the mammalian cochlea. J Neurophysiol 103:2532–2543